SCIENCE CHINA
Physics, Mechanics & Astronomy

• Article •

July 2019 Vol. 62 No. 7: 970313
https://doi.org/10.1007/s11433-018-9339-0

Ordered space-time structures: Quantum carpets from Gaussian sum theory

HuiXin Xiong[1], XueKe Song[2,3,4*], HuaiYang Yuan[2], DaPeng Yu[2,4], and ManHong Yung[2,4,5*]

[1]*Department of Physics, Peking University, Beijing 100871, China;*
[2]*Institute for Quantum Science and Engineering and Department of Physics, Southern University of Science and Technology, Shenzhen 518055, China;*
[3]*Department of Physics, Southeast University, Nanjing 211189, China;*
[4]*Shenzhen Key Laboratory of Quantum Science and Engineering, Southern University of Science and Technology, Shenzhen 518055, China;*
[5]*Central Research Institute, Huawei Technologies, Shenzhen 518129, China*

Received September 12, 2018; accepted December 5, 2018; published online March 12, 2019

The term "quantum carpet" can be observed in many closed quantum systems, where the evolution of a wave function exhibits a carpet-like pattern. Quantum carpet mechanisms are also akin to the classical interference patterns of light. Although the origins of quantum carpets have previously been studied by various researchers, many interesting details are still worth exploring. In this study, we present a unified framework for simultaneously analyzing three different features of quantum carpets: full revival, fractional revival, and diagonal canal. For the fractional revival feature, a complete formula is presented to explain its formation through Gaussian sum theory, in which all essential features, including phases and amplitudes, are captured analytically. We also reveal important relationships between the interference terms of diagonal canals and their geometric interpretations such that a better understanding of the development of diagonal canals can be supported.

quantum carpets, fractional revival, diagonal canal, Gaussian sum theory

PACS number(s): 03.65.-w, 03.65.Ge, 02.30.-f

Citation: H. X. Xiong, X. K. Song, H. Y. Yuan, D. P. Yu, and M. H. Yung, Ordered space-time structures: Quantum carpets from Gaussian sum theory, Sci. China-Phys. Mech. Astron. **62**, 970313 (2019), https://doi.org/10.1007/s11433-018-9339-0

1 Introduction

In quantum mechanics, the infinite square well, also known as the "particle-in-a-box" model, remains one of the best physical models used for illustrating the various fundamental concepts of quantum theory [1-4]. It captures the essential features of bound state problems through a deep confining potential, providing the first algebraic approximations to semiconductor quantum wells [5-7]. In terms of energies, all eigenvalues and eigenvectors of the infinite square well can be obtained analytically with the dynamics solved through the eigenstate expansion method [8-12] as well as machine learning [13,14]. Moreover, the quantum adiabatic dynamics of an infinite potential well with moving walls can be accelerated through various shortcuts to adiabaticity [15-18]. Even though the dynamics of the particles inside an infinite square well are well understood, studies continue to aspire new insights into the field of quantum physics [19-24].

The evolution of a wave function for a particle that is free to move inside an infinite square well potential exists in an art-like pattern. Such a pattern has been classified as a "quantum carpet", which was originally introduced by Kaplan et al. [25] to describe intermodal traces of individual eigenmodes that are multi-degenerate. Quantum carpets illustrate the evolution of wave functions in the space-time

*Corresponding authors (XueKe Song, email: songxk@sustc.edu.cn; ManHong Yung, email: yung@sustc.edu.cn)

continuum, revealing key features that emerge from an initial wave function after the "revival time" [26]. Essentially, the occurrence of such revival patterns in quantum carpets are owing to phase alignments in neighboring eigenstates during the evolution [27-36]. Experimentally, the properties of quantum carpets have been illustrated through a wide variety of systems, including the Rydberg atom [37], the optical lattice [38], the cavity quantum electrodynamic systems [39] and the optical waveguides [40].

Apart from a full revival of the initial wave function, the time evolution of a quantum carpet also comprises solutions that clone initial wave functions throughout the well, a phenomenon called "fractional revival" [41-44], which originates from a phase alignment with non-adjacent eigenstates. A fractional revival appears when the evolution time is fractional multiples of the revival time [45-48]. Various approaches have been developed to analyze fractional revivals. For example, previous analysis [41] has based the fractional revival on the dynamics of classical-like wave packets, in which the amplitudes and relative phase were obtained. Fourier analysis could also be applied directly to examine fractional revival [42], in which absolute phases could be obtained. However, the authors did not provide a complete account of the fractional revival in this instance with the results unable to explain the identical nature of the copied amplitudes.

Thus, the goal of our work is to present a unified framework that is capable of recovering both the revival amplitudes and absolute phases in a fractional revival, without relying on classical physics. To this end, we use a continuous quantum carpet formula to explain fractional revival using "Gaussian sum theory", where both the revival amplitudes and absolute phases can be analyzed through the same framework. Alternatively, other patterns of continuous quantum carpets exist (e.g., diagonal canals), whose formation can be explained by deconstructing a carpet into background and interference terms through the Wigner function [49, 50]. We also provide a detailed analysis on the relations between background/interference terms and their geometrical representations in the diagonal canals. Finally, we theoretically describe a discrete carpet, and then discuss its experimental application by optical waveguide.

This paper is organized as follows. In sect. 2, we analyze the general framework of continuous carpets, including the full revival, fractional revival, and diagonal canal. We then present a new formula for fractional revival with the explicit analysis of background/interference terms for the diagonal canal. In sect. 3, we attempt a theoretical investigation into discrete carpets, followed by a discussion towards its experimental implementation in optical waveguides; this is followed by a summary in sect. 4.

2 Continuous quantum carpets

2.1 Full revival of the wave function

We consider a particle with mass m trapped inside an infinite square well having a potential defined by

$$V(x) = \begin{cases} 0, & x \in (0, L), \\ \infty, & x \notin (0, L). \end{cases} \tag{1}$$

Here, the time evolution of the wave function is given by $\Psi(x,t) = \sum_{n=1}^{\infty} c_n \psi_n(x) \mathrm{e}^{-\mathrm{i}E_n t/\hbar}$, where the eigenstates are

$$\psi_n(x) = \eta_x \sqrt{\frac{2}{L}} \sin(\pi n x/L), \tag{2}$$

$\eta_x = 1$ exists if $x \in (0, L)$, otherwise $\eta_x = 0$. At the initial time, we focus on the Gaussian wave packet:

$$\Psi(x,0) = \frac{1}{\sqrt{\sqrt{2\pi} s_x}} \exp\left[-\frac{(x-\bar{x})^2}{4s_x^2}\right] \exp(\mathrm{i}\bar{p}x/\hbar) \tag{3}$$

being the initial state, where $\bar{x}$ and $\bar{p}$ are the expectation (or average) values of the position and its momentum operators, respectively. s_x is the standard deviation of the particle position. Recall that if the energy eigenvalues are represented as $E_n = n^2\pi^2\hbar^2/2mL^2$, we therefore have

$$\Psi(x,t) = \sum_{n=1}^{\infty} c_n \psi_n(x) \exp\left(-\mathrm{i}2\pi n^2 \frac{t}{4mL^2/\pi\hbar}\right). \tag{4}$$

This implies that after the period $t = T$ with

$$T = 4mL^2/\pi\hbar, \tag{5}$$

the wave function repeats itself as a full revival (i.e., $\Psi(x,T) = \Psi(x,0)$), as shown in Figure 1(a). Details of this evolution for quantum carpets at $t < 0.1T$ and $t > 0.9T$ are shown in Figure 1(b) and (c).

Apart from a full revival, a mirror revival exists for the wave function at $t = T/2$ (i.e., $\Psi(x, T/2) = -\Psi(L-x, 0)$). As can be seen in Figure 1(d), the wave packet reconstructs itself as a mirror image of the initial packet at $t = T/2$. This enables the reverse flow of time to occur such that the original impulsive event after a time evolution can be recreated [51].

2.2 Fractional revival

Apart from the full revival at $t = T$ and the mirror revival at $t = T/2$, a fractional revival is also present [41, 42, 44], which occurs at time points $t = (\alpha/\beta)(T/2)$, where α and β are coprime integers. Here, the wave function:

$$\Psi\left(x, \frac{\alpha}{\beta}\frac{T}{2}\right) = \eta_x \sqrt{\frac{2}{L}} \sum_{n=1}^{\infty} c_n \sin(\pi n x/L) \mathrm{e}^{-\mathrm{i}\pi n^2 \alpha/\beta} \tag{6}$$

can be regarded as a superposition of the initial states $\Psi(x,0)$ for $\alpha/\beta = 1/2, 1/3, 5/6$, as shown in Figure 2. Interestingly, while the number of wave packets is determined by the value of β, α can then be seen to affect the position of the wave packets.

In fact, a phenomenon that is similar to fractional revival, in the context of classical optics, is the Talbot effect (deemed the "Talbot carpet"), where an arbitrary wavefront of light

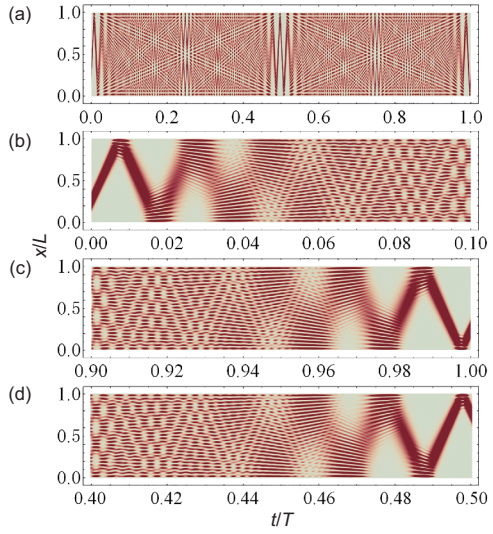

Figure 1 (Color online) A full revival and a mirror revival of the quantum carpet. x is the position of the particle, L is the width of the well, t is the evolution time, and T is the revival time. The parameters were $\bar{x}/L = 1/4$, $s_x/L = 1/(5\pi)$, $\bar{p}/(\hbar/L) = 25\pi$. The value of the probability density $|\Psi(x,t)|^2$ is color coded, where red represents a high value, and gray represents 0. (a) A plot of the quantum carpet from $t = 0$ to $t = T$. Note the reconstructed wave function $\Psi(x,t)$ at $t = T$. (b), (c) Details of the quantum carpet at $t < 0.1T$ and $t > 0.9T$. (d) A mirror image of the initial state formed at $t = T/2$.

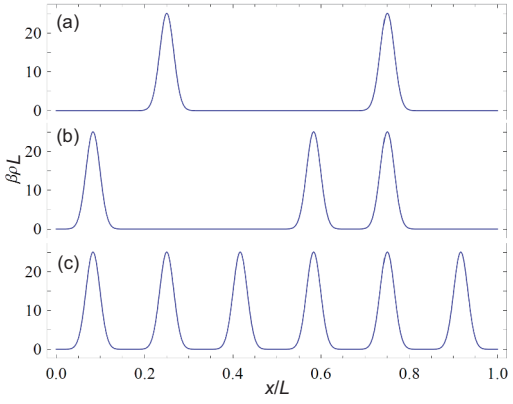

Figure 2 (Color online) The fractional revival at $\alpha/\beta = 1/2, 1/3, 5/6$ ($\alpha = 1, 1, 5$ and $\beta = 2, 3, 6$) for (a), (b), and (c). x is the position of the particle, L is the width of the well, and $\rho = |\Psi(x,t)|^2$ is the probability distribution, where $t = (\alpha/\beta)(T/2)$ and T is the revival time, respectively. The other parameters are $\bar{x}/L = 1/4$, $s_x/L = 1/(20\pi)$ and $\bar{p}/(\hbar/L) = 25\pi$. We find that the number of wave packets are identical to the value of β.

reconstructs itself to produce different gratings of different sizes much like a superposition of several initial wavefronts. This traversed well with the "Gaussian sum theory" [26]. Owing to this comparison, a new fractional carpet formula, simultaneously containing revival amplitudes and absolute phases, is given here through a Gaussian sum. In particular, the wave function, in this case, is a superposition of the oddly extended initial state $\Phi(x,0)$, where the odd extension means that

$$\Phi(x,t) = \sum_{n=-\infty}^{\infty} \tilde{\Psi}(x - 2Ln, t), \tag{7}$$

and

$$\tilde{\Psi}(x,t) = \Psi(x,t) - \Psi(-x,t). \tag{8}$$

There are β copies of $\Phi(x,0)$ in the fractional revival. And each of the copies contributes only one initial packet $\Psi(x,0)$ to the revival.

To create a fractional revival, we write the expansion coefficient as:

$$c_n = \sqrt{2/L} \int_0^L \sin(\pi n x/L)\, \tilde{\Psi}(x,0)\, \mathrm{d}x\,. \tag{9}$$

Using the identity $\sin\theta = \left(\mathrm{e}^{\mathrm{i}\theta} - \mathrm{e}^{-\mathrm{i}\theta}\right)/2\mathrm{i}$, this can be rearranged as:

$$c_n = \frac{1}{2\mathrm{i}} \sqrt{\frac{2}{L}} \int_{-\infty}^{\infty} \mathrm{e}^{\mathrm{i}\pi n x/L} \tilde{\Psi}(x,0)\, \mathrm{d}x. \tag{10}$$

Let us now extend the definition of c_n for $n = 0, \pm1, \pm2, \pm3$, such that $c_{-n} = -c_n$. Hence

$$\Psi\left(x, \frac{\alpha}{\beta}\frac{T}{2}\right) = \frac{\eta_x}{2\mathrm{i}} \sqrt{\frac{2}{L}} \sum_{n=-\infty}^{\infty} c_n \mathrm{e}^{\mathrm{i}\pi n x/L} \mathrm{e}^{-\mathrm{i}\pi n^2 \alpha/\beta}. \tag{11}$$

If we substitute eq. (10) into eq. (11) whilst switching the order between summation and integration, we obtain

$$\Psi(x,t) = \frac{\eta_x}{2L} \int_{-\infty}^{\infty} \tilde{\Psi}(x',0) \times \left[\sum_{n=-\infty}^{\infty} f(n)\right] \mathrm{d}x', \tag{12}$$

where $f(n) \equiv \exp\left(\mathrm{i}\pi n \frac{x-x'}{L}\right) \exp\left(-\mathrm{i}\pi n^2 \frac{\alpha}{\beta}\right)$. By introducing the symbol q_α, where $q_\alpha = 1$ if α is odd and $q_\alpha = 0$ if α is even, this expression can be simplified to

$$\Psi\left(x, \frac{\alpha}{\beta}\frac{T}{2}\right) = \frac{\eta_x}{\beta} \sum_{n=-\infty}^{\infty} \tilde{\Psi}(x - Lq_\alpha - 2Ln/\beta, 0)\, S(n,\alpha,\beta)\,, \tag{13}$$

(see the details in Appendix A), where $S(n,\alpha,\beta) = \sum_{j=1}^{\beta} \exp\left[\mathrm{i}\pi j (q_\alpha + 2n/\beta - j\alpha/\beta)\right]$ is the Gaussian sum [26]. In number theory [52], for any integer n and any coprime integer α and β, we use

$$|S(n,\alpha,\beta)| = \sqrt{\beta}, \tag{14}$$

which implies that

$$S(n,\alpha,\beta) = \sqrt{\beta}\exp\left[\mathrm{i}\Theta(n,\alpha,\beta)\right], \tag{15}$$

where, $\Theta(n,\alpha,\beta) = \arg S(n,\alpha,\beta)$. By substituting eq. (15) into eq. (13), and using $\Theta(\beta n + j,\alpha,\beta) = \Theta(j,\alpha,\beta)$, which can be derived easily from its definition, we then get

$$\Psi\left(x,\frac{\alpha}{\beta}\frac{T}{2}\right) = \frac{\eta_x}{\sqrt{\beta}}\sum_{n=-\infty}^{\infty}\sum_{j=1}^{\beta}\tilde{\Psi}(x - Lq_\alpha - 2Lj/\beta - 2Ln, 0) \times \exp\left[\mathrm{i}\Theta(j,\alpha,\beta)\right]. \tag{16}$$

If we switch the order between summations, we finally get

$$\Psi\left(x,\frac{\alpha}{\beta}\frac{T}{2}\right) = \frac{\eta_x}{\sqrt{\beta}}\sum_{n=1}^{\beta}\Phi(x - Lq_\alpha - 2Ln/\beta, 0) \times \exp\left[\mathrm{i}\Theta(n,\alpha,\beta)\right], \tag{17}$$

where $\Theta(n,\alpha,\beta)$ is the absolute phase and $1/\sqrt{\beta}$ is the equivalent amplitude; both are analytically given at the same time. The relative phase can be obtained through a difference between absolute phases. For any initial state $\Psi(x,0)$, the wave function $\Psi(x,t)$ depicts the fractional revival at time $t = (\alpha/\beta)(T/2)$. Is a superposition of β copies of the oddly extended initial wave packet $\Phi(x,0)$, which are separated by $2L/\beta$ in the x coordinate.

If copies of the extended initial wave packet $\Phi(x,0)$ does not overlap, the fractional revival then resembles separate wave packets, as shown in Figure 2. If they do overlap, interference patterns will start to form, as shown in Figure 3. The maximum number of initial wave packets from a fractional revival is therefore limited by the width of the packet.

2.3 Diagonal canals

Here, the diagonal canal produced refers to the group of gray lines that traverse the carpet from each side, similar to the green lines shown in Figure 4(a). This phenomenon can be explained by deconstructing the quantum carpet back into basic background and interference terms using the Wigner function $W_f(x,p,t)$ [49], which is defined as:

$$W_f = \frac{1}{\pi\hbar}\int_{-\infty}^{\infty} f^*(x+y,t)\,f(x-y,t)\,\mathrm{e}^{2\mathrm{i}py/\hbar}\mathrm{d}y, \tag{18}$$

where $f(x,t)$ is an arbitrary function of the variables x and t.

From eqs. (18) and (7), we obtain

$$W_\Phi(x,p,t) = \frac{1}{\pi\hbar}\sum_{j,k=-\infty}^{\infty}\int_{-\infty}^{\infty}\tilde{\Psi}^*(x+y-2Lj,t) \times \tilde{\Psi}(x-y-2Lk,t)\,\mathrm{e}^{2\mathrm{i}py/\hbar}\mathrm{d}y. \tag{19}$$

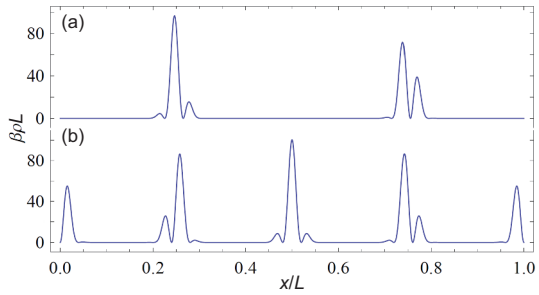

Figure 3 (Color online) A fractional revival at $\alpha/\beta = 3/4, 3/8$ for (a) and (b). Here x is the position of the particle, L is the width of the well, $\rho = |\Psi(x,t)|^2$ is the probability distribution where $t = (\alpha/\beta)(T/2)$, and T is the revival time. The other parameters $\bar{x}$, s_x, $\bar{p}$ are the same as Figure 2. Note that there are interference patterns observed as the superposed wave functions overlap.

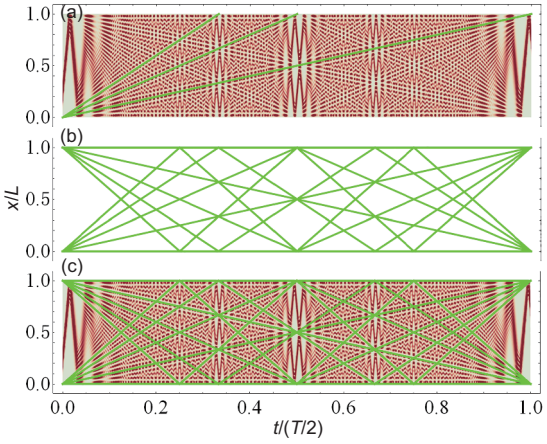

Figure 4 (Color online) The diagonal canals crisscrossing the quantum carpet. The color code and associated parameters $\bar{x}$, s_x, $\bar{p}$ are the same as those in Figure 1. (a) Three diagonal canals of the quantum carpet are emphasized using green lines. (b) Straight lines that satisfy $\tilde{x} = 0$. Integer j obtained between -4 and 4 and integer k between $-|j|$ and $|j|+1$. (c) A combination of (a) and (b) showing the center of grouped parallel canals (in green).

To simplify the notations, we define variables $\tilde{x}$ and $\tilde{p}$ as being

$$\tilde{x} = \left(\frac{x}{L} - j\frac{t}{T/2} - k\right)L, \quad \tilde{p} = \frac{\pi\hbar}{2L}j, \tag{20}$$

where j and k are integers. In fact, we shall see later that every straight line in the x-t plane satisfying $\tilde{x} = 0$ is the center of a group of parallel canals, as shown in Figure 4(b) and (c). After several mathematical transformations (see Appendix B for details), eq. (19) can then be modified as:

$$W_\Phi(x,p,t) = \frac{\pi\hbar}{2L}\sum_{j,k=-\infty}^{\infty}(-1)^{jk}W_{\tilde{\Psi}}(x - Lk, p, t)\,\delta(p - \tilde{p}). \tag{21}$$

There are two useful properties the of Wigner function that can be derived from its definition. First, $|f|^2$ can be ob-

tained using $|f|^2 = \int_{-\infty}^{\infty} W_f \mathrm{d}p$. Second, if the given function f satisfies the time-dependent Schrödinger equation of a free particle $\mathrm{i}\hbar\frac{\partial}{\partial t}f = -\frac{\hbar^2}{2m}\frac{\partial^2}{\partial x^2}f$ with boundary conditions $f(x \to \pm\infty, t) = 0$, then the time evolution of the Wigner function can be written as $W_f(x,p,t) = W_f\left(x - \frac{p}{m}t, p, 0\right)$. We observe that $|\Psi(x,t)|^2 = \eta_x|\Phi(x,t)|^2$, which suggests that $|\Psi(x,t)|^2 = \eta_x\int_{-\infty}^{\infty} W_\Phi(x,p,t)\,\mathrm{d}p$. This then equates to

$$|\Psi(x,t)|^2 = \eta_x\frac{\pi\hbar}{2L}\sum_{j,k=-\infty}^{\infty}(-1)^{jk}W_{\tilde{\Psi}}(x - Lk, \tilde{p}, t). \tag{22}$$

Using the secondary properties of the Wigner function, we obtain

$$|\Psi(x,t)|^2 = \eta_x\frac{\pi\hbar}{2L}\sum_{j,k=-\infty}^{\infty}(-1)^{jk}W_{\tilde{\Psi}}(\tilde{x}, \tilde{p}, 0). \tag{23}$$

By substituting eq. (8) into the equation above, the probability density $|\Psi(x,t)|^2$, which characterizes the quantum carpet, can be further deconstructed into basic background and interference terms [49]:

$$|\Psi(x,t)|^2 = \eta_x\frac{\pi\hbar}{2L}\sum_{j,k=-\infty}^{\infty}\left(B_{j,k}^{+} + B_{j,k}^{-} + I_{j,k}\right). \tag{24}$$

This deconstruction can always be achieved regardless of the form of the initial state $\Psi(x,0)$. The background terms $B_{j,k}^{\pm}$ can be expressed by the Wigner function of the initial state $\Psi(x,0)$ as $B_{j,k}^{\pm} = (-1)^{jk}W_\Psi(\pm\tilde{x}, \pm\tilde{p}, 0)$. The interference terms $I_{j,k} = (-1)^{jk}I(\tilde{x}, \tilde{p}, 0)$ can also be obtained from $I(x,p,t) = W_{\tilde{\Psi}}(x,p,t) - W_\Psi(x,p,t) - W_\Psi(-x,-p,t)$.

In our calculations, the initial state $\Psi(x,0)$ is eq. (3), such that the specific expressions for $B_{j,k}^{\pm}$ and $I_{j,k}$ are

$$B_{j,k}^{\pm} = \frac{(-1)^{jk}}{\pi\hbar}G\left(\frac{\pm\tilde{x} - \bar{x}}{s_x}\right)G\left(\frac{\pm\tilde{p} - \bar{p}}{s_p}\right) \tag{25}$$

and

$$I_{j,k} = -2\frac{(-1)^{jk}}{\pi\hbar}G\left(\frac{\tilde{x}}{s_x}\right)G\left(\frac{\tilde{p}}{s_p}\right)\cos\left(\frac{\bar{x}\tilde{p} - \bar{p}\tilde{x}}{\hbar/2}\right), \tag{26}$$

where G is defined as $G(\theta) = \exp\left(-\theta^2/2\right)$. The oscillation of interference terms $I_{j,k}$ comes from the "cos" factor in eq. (26), which depends on the variables $\tilde{x}$ and $\tilde{p}$.

An analysis of the relationship between background and interference terms and their corresponding geometries are given in Figures 5 and 6 with the notations $\sum_\theta = \sum_{\theta=-\infty}^{\infty}$. $B_{j,k}^{+}$ propagates in the direction of $\bar{p}$ whilst $B_{j,k}^{-}$ propagates against, as shown in Figure 5(a) and (b). The total background can be obtained using $\sum_{j,k}B_{j,k}^{+} + \sum_{j,k}B_{j,k}^{-}$ (Figure 5(c)). In fact, only the terms $\sum_j B_{j,k}^{\pm}$ with even k will contribute to the total background. Conversely, the sum $\sum_j B_{j,k}^{\pm}$ will oscillate to 0 if k is odd due to the factor $(-1)^{jk}$ in $B_{j,k}^{\pm}$. As shown in Figure 5(d),

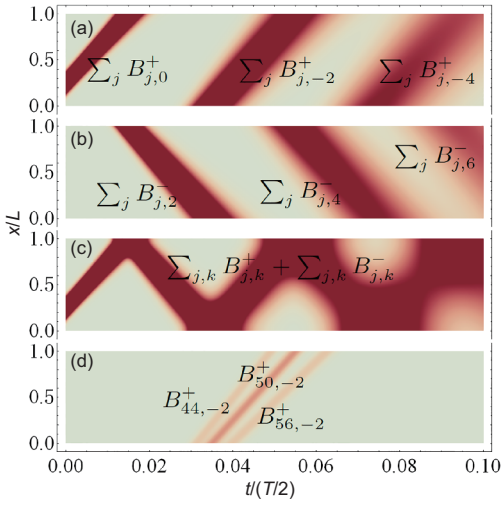

Figure 5 (Color online) Geometry ascribed to the background terms. The color code and associated parameters $\bar{x}$, s_x, $\bar{p}$ are the same as those in Figure 1. (a) $B_{j,k}^{+}$ propagates toward the $\bar{p}$ direction. $\sum_j B_{j,0}^{+}$, $\sum_j B_{j,-2}^{+}$, and $\sum_j B_{j,-4}^{+}$ are shown from left to right. (b) $B_{j,k}^{-}$ propagates against the direction of $\bar{p}$. $\sum_j B_{j,2}^{-}$, $\sum_j B_{j,4}^{-}$, and $\sum_j B_{j,6}^{-}$ are shown from left to right. (c) The total background obtained using $\sum_{j,k}B_{j,k}^{+} + \sum_{j,k}B_{j,k}^{-}$. (d) The summation over j leads to the spread of wave packet. $B_{44,-2}^{+}$, $B_{50,-2}^{+}$ and $B_{56,-2}^{+}$ are shown from left to right.

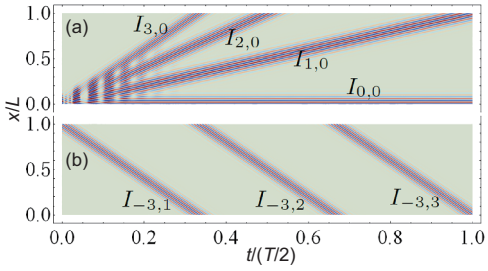

Figure 6 (Color online) Geometry ascribed to the interference terms. The color code and associated parameters $\bar{x}$, s_x, $\bar{p}$ are the same as those in Figure 1. Here, negative values are represented in blue. (a) The slope of the interference term $I_{j,k}$ depends on the integer j. $I_{0,0}$, $I_{1,0}$, $I_{2,0}$, and $I_{3,0}$ are displayed from bottom to top. Each term is centered along straight line $\tilde{x} = 0$, where $j = 0, 1, 2, 3$ and $k = 0$. (b) The intercept of $I_{j,k}$ showing its dependence on integer k. $I_{-3,1}$, $I_{-3,2}$, and $I_{-3,3}$ are displayed from left to right. Each term is centered along straight line $\tilde{x} = 0$, where $j = -3$ and $k = 1, 2, 3$.

the sum over j leads to the spread of the wave packet.

Moreover, it is quite clear to get the corresponding geometries of interference terms. Every $I_{j,k}$ digs several parallel canals along straight line $\tilde{x} = 0$ with different slope controlled by j (shown in Figure 6(a)) and intercept controlled by k (shown in Figure 6(b)).

3 Discrete quantum carpets

3.1 Theoretical analysis

Let $|1\rangle, |2\rangle, ..., |N\rangle$ be a complete set of orthogonal projectors for a quantum system. A Hamiltonian composed of nearest-

neighbor two-body interactions then takes the form of

$$\hat{H} = -\frac{J}{2}\sum_{n=1}^{N-1}\left(|n+1\rangle\langle n| + |n\rangle\langle n+1|\right), \tag{27}$$

where J represents the coupling strength. This Hamiltonian is equivalent to infinite-square-well if the basis $|1\rangle, |2\rangle, ..., |N\rangle$ are regarded as position eigenstates and their total number N is large enough. The discrete version of the initial state of eq. (3) is

$$|\Psi_0\rangle = A\sum_{n=1}^{N}\exp\left[-\frac{(x_n-\bar{x})^2}{4s_x^2}\right]\exp\left(\mathrm{i}\bar{p}x_n/\hbar\right)|n\rangle, \tag{28}$$

where $A = \left[\sum_{n=1}^{N} G\left(\left(x_n-\bar{x}\right)/s_x\right)\right]^{-1/2}$ is the normalization coefficient and $x_n = nL/N$ are points equally spaced in the discrete well. By solving the dynamic Schrödinger equation $\mathrm{i}\hbar\frac{\partial}{\partial t}|\Psi\rangle = \hat{H}|\Psi\rangle$ through the initial conditions proposed in eq. (28), we get the time-dependent state:

$$|\Psi_t\rangle = \hat{U}^{\dagger}\hat{D}\hat{U}|\Psi_0\rangle, \tag{29}$$

where the operator $\hat{U}$ is unitary with matrix elements:

$$\langle j|\hat{U}|k\rangle = \sqrt{\frac{2}{N+1}}\sin\left(\pi\frac{jk}{N+1}\right). \tag{30}$$

The operator $\hat{D}$ is diagonal with matrix elements:

$$\langle n|\hat{D}|n\rangle = \exp\left(-\mathrm{i}\varepsilon_n t/\hbar\right), \tag{31}$$

where ε_n are the energy eigenvalues such that

$$\varepsilon_n = -J\cos\left(\pi\frac{n}{N+1}\right). \tag{32}$$

A numerical calculation of the discrete carpet $|\langle n\,|\,\Psi_t\rangle|^2$, where $N = 150$, is given in Figure 7(a) with the horizontal coordinate t and vertical coordinate n. It shows the same behavior with the continuous one (Figure 7(b)).

3.2 Experimental methods

A reasonable way to observe a discrete carpet is through a waveguide array, as shown in Figure 8. Here, a photon propagates into a waveguide array through N single-mode channels that are parallel to each other. The latter can be described by position eigenstates $|1\rangle, |2\rangle, \ldots, |N\rangle$, where $|n\rangle$ represents a photon cited within the array at $x_n = nL/N$. The gap between these waveguides make it possible to overlap individual modes. In this case, the waves propagating between

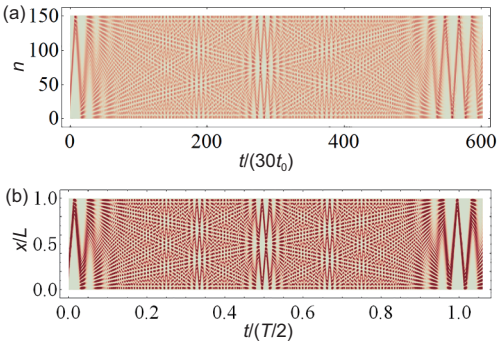

Figure 7 (Color online) A comparison of the discrete quantum carpet (a) and the continuous quantum carpet (b). The color code and associated parameters $\bar{x}$, s_x, $\bar{p}$ are the same as those in Figure 1. Here, n is the position eigenstate $|n\rangle$, t is the evolution time, t_0 is a time unit defined by $t_0 = \hbar/J$, and T is the notation given by eq. (5).

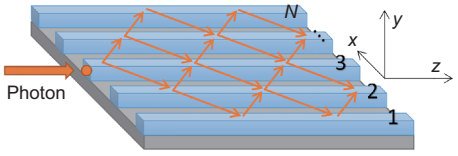

Figure 8 (Color online) An example of a waveguide array showing a photon propagating in the x-z plane to form a carpet.

waveguides (in the x direction) satisfy the Hamiltonian in eq. (27) [53]. To observe quantum carpets, we manipulate the wave length of the photon and the space between waveguides. By doing this, the quantum carpets appear as the two experimental parameters have the ability to make single-mode waveguides overlap.

In the z direction, propagating photons along waveguides occurs through uniform motion, which transforms the time evolution into a space variation. Here, we are able to input the same initial state at $z = 0$ to detect the photon at $z = z_i$. Through the statistical distribution of photons, the discrete quantum carpet at a given moment $t = z_i/c$ is obtainable, where c is the speed of light in the medium. By combining each of the distributions at $z_1, z_2, z_3, ...$ together, we can therefore obtain the experimental discrete quantum carpet.

As shown in Figure 7, $N = 150$ is sufficient to observe a clear pattern of carpet while the experiments can couple waveguides up to 10^4 channels [54], which can fully satisfy the requirement.

4 Summary

In this study, we have analyzed three essential features of continuous (i.e., full revival, fractional revival and diagonal canal) and discrete quantum carpets. For the fractional revival feature, we have interpreted this as a superposition of several oddly extended wave packets with the

same amplitude. Their absolute phases were also obtained from Gaussian sum theory. The relationships between background/interference terms of diagonal canals and their geometric representations were analyzed explicitly. The sum of background terms forms the spread, reconstruction, and reflection of wave packets, and each interference term constituted several parallel canals within the carpet. With regard to the discrete carpet, we proposed a method to experimentally observe this phenomenon using current optical waveguide technology. Overall, we believe our results improved the understanding between the fundamental "particle in box" model and intricate quantum carpet patterns.

This work was supported by the National Natural Science Foundation of China (Grant No. 11875160), the National Natural Science Foundation of China-Guangdong Joint Fund (Grant No. U1801661), the Guangdong Innovative and Entrepreneurial Research Team Program (Grant No. 2016ZT06D348), the Natural Science Foundation of Guangdong Province (Grant No. 2017B030308003), and the Science, Technology and Innovation Commission of Shenzhen Municipality (Grant Nos. JCYJ20170412152620376, JCYJ20170817105046702, and ZDSYS201703031659262), and the Postdoctoral Science Foundation of China (Grant No. 2018M632195).

1 G. Bonneau, J. Faraut, and G. Valent, Am. J. Phys. **69**, 322 (2001).
2 R. Robinett, Phys. Rep. **392**, 1 (2004).
3 O. Fojón, M. Gadella, and L. P. Lara, Comput. Math. Appl. **59**, 964 (2010).
4 M. Waegell, Y. Aharonov, and T. Patti, Entropy **18**, 149 (2016), arXiv: 1604.05385.
5 G. Bastard, Superlattices Microstruct. **1**, 265 (1985).
6 A. S. Polkovnikov, and G. G. Zegrya, Phys. Rev. B **58**, 4039 (1998).
7 L. V. Kotova, V. N. Kats, A. V. Platonov, V. P. Kochereshko, R. André, and L. E. Golub, Phys. Rev. B **97**, 125302 (2018), arXiv: 1711.10334.
8 L. I. Schif, *Quantum Mechanics* (McGraw-Hill Book Company, New York, 1968).
9 D. J. Griffiths, *Introduction to Quantum Mechanics* (Cambridge University Press, Cambridge, 2005).
10 K. Cai, R. X. Wang, Z. Q. Yin, and G. L. Long, Sci. China-Phys. Mech. Astron. **60**, 070311 (2017), arXiv: 1610.09922.
11 H. Y. Yuan, M. H. Yung, and X. R. Wang, Phys. Rev. B **98**, 060407 (2018), arXiv: 1801.09017.
12 H. Y. Yuan, and M. H. Yung, Phys. Rev. B **97**, 060405 (2018), arXiv: 1711.04394.
13 K. Mills, M. Spanner, and I. Tamblyn, Phys. Rev. A **96**, 042113 (2017).
14 Y. B. Sheng, and L. Zhou, Sci. Bull. **62**, 1025 (2017).
15 X. Chen, I. Lizuain, A. Ruschhaupt, D. Guéry-Odelin, and J. G. Muga, Phys. Rev. Lett. **105**, 123003 (2010), arXiv: 1003.2515.
16 A. Campo, and M. G. Boshier, Sci. Rep. **2**, 648 (2012), arXiv: 1201.6627.
17 X. K. Song, H. Zhang, Q. Ai, J. Qiu, and F. G. Deng, New J. Phys. **18**, 023001 (2016), arXiv: 1509.00097.
18 X. K. Song, Q. Ai, J. Qiu, and F. G. Deng, Phys. Rev. A **93**, 052324 (2016), arXiv: 1602.00050.
19 S. Iqbal, and F. Saif, J. Russ. Laser Res. **29**, 466 (2008).
20 Y. B. Sheng, and L. Zhou, Sci. Rep. **5**, 7815 (2015).
21 Y. B. Sheng, and L. Zhou, Phys. Rev. A **98**, 052343 (2018).
22 M. Belloni, and R. W. Robinett, Phys. Rep. **540**, 25 (2014).
23 C.-L. Lin, arXiv: 1604.04680.
24 C.-L. Lin, arXiv: 1705.05517.
25 A. E. Kaplan, I. Marzoli, W. E. Lamb, and W. P. Schleich, Phys. Rev. A **61**, 032101 (2000).
26 M. Berry, I. Marzoli, and W. Schleich, Phys. World **14**, 39 (2001).
27 M. Nest, Phys. Rev. A **73**, 023613 (2006).
28 K. Hornberger, S. Gerlich, P. Haslinger, S. Nimmrichter, and M. Arndt, Rev. Mod. Phys. **84**, 157 (2012), arXiv: 1109.5937.
29 M. H. Muñoz-Arias, J. Madroñero, and C. A. Parra-Murillo, Phys. Rev. A **93**, 043603 (2016), arXiv: 1512.06716.
30 M. R. Barros, A. Ketterer, O. J. Farías, and S. P. Walborn, Phys. Rev. A **95**, 042311 (2017), arXiv: 1702.07391.
31 I. Yousaf, and S. Iqbal, J. Russ. Laser Res. **37**, 328 (2016).
32 P. Kazemi, S. Chaturvedi, I. Marzoli, R. F. O'Connell, and W. P. Schleich, New J. Phys. **15**, 013052 (2013).
33 T. García, N. A. Cordero, and E. Romera, Phys. Rev. B **89**, 075416 (2014).
34 L. Banchi, E. Compagno, and S. Bose, Phys. Rev. A **91**, 052323 (2015), arXiv: 1502.03061.
35 M. Rohith, and C. Sudheesh, Phys. Rev. A **92**, 053828 (2015), arXiv: 1507.03724.
36 M. Krizanac, D. Altwein, E. Y. Vedmedenko, and R. Wiesendanger, New J. Phys. **18**, 033029 (2016), arXiv: 1601.00803.
37 J. A. Yeazell, M. Mallalieu, and C. R. Stroud, Phys. Rev. Lett. **64**, 2007 (1990).
38 M. Greiner, O. Mandel, T. W. Hänsch, and I. Bloch, Nature **419**, 51 (2002).
39 G. Rempe, H. Walther, and N. Klein, Phys. Rev. Lett. **58**, 353 (1987).
40 G. Della Valle, M. Savoini, M. Ornigotti, P. Laporta, V. Foglietti, M. Finazzi, L. Duò, and S. Longhi, Phys. Rev. Lett. **102**, 180402 (2009).
41 D. L. Aronstein, and C. R. Stroud, Phys. Rev. A **55**, 4526 (1997).
42 K. R. Naqvi, S. Waldenstrøm, and T. H. Hassan, Eur. J. Phys. **22**, 395 (2001).
43 M. Spanner, E. A. Shapiro, and M. Ivanov, Phys. Rev. Lett. **92**, 093001 (2004).
44 P. A. Bernard, A. Chan, Loranger, C. Tamon, and L. Vinet, Phys. Lett. A **382**, 259 (2018), arXiv: 1710.02705.
45 S. Dooley, and T. P. Spiller, Phys. Rev. A **90**, 012320 (2014), arXiv: 1404.4296.
46 M. Rohith, and C. Sudheesh, J. Phys. B-At. Mol. Opt. Phys. **47**, 045504 (2014), arXiv: 1309.0104.
47 J. M. Lemay, L. Vinet, and A. Zhedanov, J. Phys. A-Math. Theor. **49**, 335302 (2016), arXiv: 1509.08965.
48 M. Christandl, L. Vinet, and A. Zhedanov, Phys. Rev. A **96**, 032335 (2017), arXiv: 1607.02639.
49 P. Stifter, C. Leichtie, W. P. Schleich, and J. Marklof, Z. Naturforschung A **52**, 377 (1997).
50 O. M. Friesch, I. Marzoli, and W. P. Schleich, New J. Phys. **2**, 4 (2000).
51 K. Lin, P. Lu, J. Ma, X. Gong, Q. Song, Q. Ji, W. Zhang, H. Zeng, J. Wu, G. Karras, G. Siour, J. M. Hartmann, O. Faucher, E. Gershnabel, Y. Prior, and I. S. Averbukh, Phys. Rev. X **6**, 041056 (2016), arXiv: 1606.08200.
52 T. M. Apostol, *Introduction to Analytic Number Theory* (Springer, New York, 1976).
53 D. N. Christodoulides, F. Lederer, and Y. Silberberg, Nature **424**, 817 (2003).
54 H. B. Perets, Y. Lahini, F. Pozzi, M. Sorel, R. Morandotti, and Y. Silberberg, Phys. Rev. Lett. **100**, 170506 (2008), arXiv: 0707.0741.
55 A. Deitmar, and S. Echterhoff, *Principles of Harmonic Analysis* (Springer, New York, 2009).

Appendix A Deconstructing the summation

Note that we are able to divide $\sum_{n=-\infty}^{\infty} f(n) = \sum_{n=-\infty}^{\infty} \sum_{j=1}^{\beta} f(\beta n + j)$ into groups. For example, if $\beta = 3$, then $+ f(-2) + f(-1) + f(0) + f(1) + f(2) + f(3) + f(4) +$

$f(5)+f(6)+\ =\ +[f(-2)+f(-1)+f(0)]+[f(1)+f(2)+f(3)]+[f(4)+f(5)+f(6)]+$. In this way, we form

$$\begin{aligned}&\sum_{n=-\infty}^{\infty}\exp\left(\mathrm{i}\pi n\frac{x-x'}{L}\right)\exp\left(-\mathrm{i}\pi n^2\frac{\alpha}{\beta}\right)\\&=\left\{\sum_{n=-\infty}^{\infty}\exp\left[\mathrm{i}\pi n\beta\left(\frac{x-x'}{L}-q_\alpha\right)\right]\right\}\\&\quad\times\left\{\sum_{j=1}^{\beta}\exp\left[\mathrm{i}\pi j\left(\frac{x-x'}{L}-j\frac{\alpha}{\beta}\right)\right]\right\},\end{aligned}\tag{a1}$$

where $q_\alpha = 1$ if α exists as an odd number and $q_\alpha = 0$ if α exists as an even number. If we use the ordinary Poisson summation formula [55]:

$$\sum_{n=-\infty}^{\infty}\mathrm{e}^{\mathrm{i}2\pi n\theta}=\sum_{n=-\infty}^{\infty}\delta(n-\theta),\tag{a2}$$

with δ as the Dirac delta function, the expression in eq. (a1) can be given by

$$\frac{2L}{\beta}\sum_{n=-\infty}^{\infty}\sum_{j=1}^{\beta}\delta(\kappa)\exp\left[\mathrm{i}\pi j\left(q_\alpha+\frac{2n-j\alpha}{\beta}\right)\right],\tag{a3}$$

where $\kappa = x-x'-Lq_\alpha-2Ln/\beta$. If we substitute eq. (a3) into eq. (12), and switch the order between summation and integration, we then obtain eq. (13).

Appendix B Pattern decomposition

For the Wigner function:

$$\begin{aligned}W_\Phi(x,p,t)=&\frac{1}{\pi\hbar}\sum_{j,k=-\infty}^{\infty}\int_{-\infty}^{\infty}\tilde{\Psi}^*(x+y-2Lj,t)\\&\times\tilde{\Psi}(x-y-2Lk,t)\,\mathrm{e}^{2\mathrm{i}py/\hbar}\mathrm{d}y.\end{aligned}\tag{a4}$$

If we replace y by $y = z+2Lj$ and switch the order in the summation to

$$\sum_{j,k=-\infty}^{\infty}f(j,k)=\sum_{j,k=-\infty}^{\infty}f(j,k-j),\tag{a5}$$

we get

$$\begin{aligned}W_\Phi(x,p,t)=&\frac{1}{\pi\hbar}\left(\sum_{j=-\infty}^{\infty}\mathrm{e}^{4\mathrm{i}pLj/\hbar}\right)\sum_{k=-\infty}^{\infty}\int_{-\infty}^{\infty}\tilde{\Psi}^*(x+z,t)\\&\times\tilde{\Psi}(x-z-2Lk,t)\,\mathrm{e}^{2\mathrm{i}pz/\hbar}\mathrm{d}z.\end{aligned}\tag{a6}$$

By using the ordinary Poisson summation formula (a2) and replace z with $z = y-Lk$, we have

$$W_\Phi(x,p,t)=\frac{\pi\hbar}{2L}\sum_{j,k=-\infty}^{\infty}(-1)^{jk}W_{\tilde{\Psi}}(x-Lk,p,t)\,\delta(p-\tilde{p}).\tag{a7}$$

This then becomes

$$|\Psi(x,t)|^2=\eta_x\frac{\pi\hbar}{2L}\sum_{j,k=-\infty}^{\infty}(-1)^{jk}W_{\tilde{\Psi}}(x-Lk,\tilde{p},t).\tag{a8}$$

From $\tilde{\Psi}(\pm\infty,t)=0$, $\mathrm{i}\hbar\frac{\partial}{\partial t}\tilde{\Psi}(x,t)=-\frac{\hbar^2}{2m}\frac{\partial^2}{\partial x^2}\tilde{\Psi}(x,t)$, and the eq. (a8), we obtain

$$|\Psi(x,t)|^2=\eta_x\frac{\pi\hbar}{2L}\sum_{j,k=-\infty}^{\infty}(-1)^{jk}W_{\tilde{\Psi}}(\tilde{x},\tilde{p},0).\tag{a9}$$

By substituting eq. (8) into eq. (a9), we find that

$$\begin{aligned}|\Psi(x,t)|^2=&\eta_x\frac{\pi\hbar}{2L}\sum_{j,k=-\infty}^{\infty}(-1)^{jk}\times[W_\Psi(\tilde{x},\tilde{p},0)\\&+W_\Psi(-\tilde{x},-\tilde{p},0)+I(\tilde{x},\tilde{p},0)],\end{aligned}\tag{a10}$$

where

$$\begin{aligned}I(x,p,t)=&W_{\tilde{\Psi}}(x,p,t)-W_\Psi(x,p,t)-W_\Psi(-x,-p,t)\\=&-\frac{2}{\pi\hbar}\mathrm{Re}\int_{-\infty}^{\infty}\Psi^*(x+y,t)\Psi(-x+y,t)\,\mathrm{e}^{2\mathrm{i}py/\hbar}\mathrm{d}y.\end{aligned}\tag{a11}$$

If we define the background and interference terms as $B^{\pm}_{j,k}=(-1)^{jk}W_\Psi(\pm\tilde{x},\pm\tilde{p},0)$ and $I_{j,k}=(-1)^{jk}I(\tilde{x},\tilde{p},0)$, we finally yield

$$|\Psi(x,t)|^2=\eta_x\frac{\pi\hbar}{2L}\sum_{j,k=-\infty}^{\infty}\left(B^{+}_{j,k}+B^{-}_{j,k}+I_{j,k}\right).\tag{a12}$$